Patient Safety Starts Here

"If you were to purchase a 3D Scanning System today, which would you choose?"

When asked this question by a 2016 MEDPHYS Mailing List survey, the majority of respondents chose the 3D SCANNER™ from Sun Nuclear. More than 550 facilities worldwide agree—the 3D SCANNER is their preferred water tank for accurate and efficient commissioning.

Visit sunnuclear.com to learn about these advantages and more.

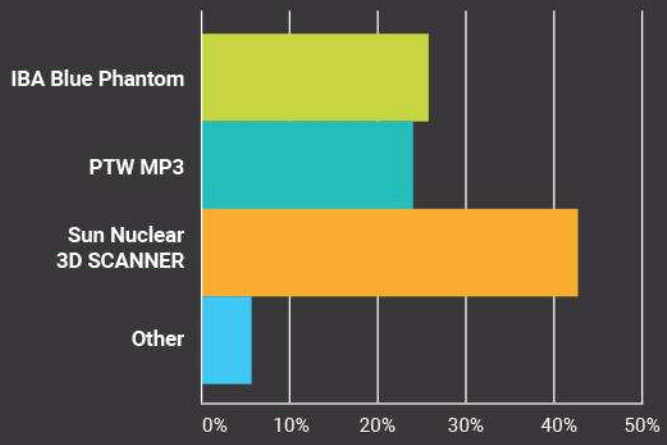

SUN NUCLEAR corporation

Technical Note: Diffusion-weighted MRI with minimal distortion in head-and-neck radiotherapy using a turbo spin echo acquisition method

Tim Schakel[a)]
Department of Radiotherapy, University Medical Center Utrecht, Heidelberglaan 100, 3584 CX Utrecht, The Netherlands

Johannes M. Hoogduin
Department of Radiology, University Medical Center Utrecht, Heidelberglaan 100, 3584 CX Utrecht, The Netherlands

Chris H.J. Terhaard and Marielle E.P. Philippens
Department of Radiotherapy, University Medical Center Utrecht, Heidelberglaan 100, 3584 CX Utrecht, The Netherlands

(Received 26 July 2016; revised 18 May 2017; accepted for publication 18 May 2017; published 30 June 2017)

Purpose: Diffusion-weighted (DW) MRI, showing high contrast between tumor and background tissue, is a promising technique in radiotherapy for tumor delineation. However, its use for head-and-neck patients is hampered by poor geometric accuracy in conventional echo planar imaging (EPI) DW-MRI. An alternative turbo spin echo sequence, DW-SPLICE, is implemented and demonstrated in patients.
Methods: The DW-SPLICE sequence was implemented on a 3.0 T system and evaluated in 10 patients. The patients were scanned in treatment position, using a customized head support and immobilization mask. Image distortions were quantified at the gross tumor volume (GTV) using field map analysis. The apparent diffusion coefficient (ADC) was evaluated using an ice water phantom.
Results: The DW images acquired by DW-SPLICE showed no image distortions. Field map analysis at the gross tumor volumes resulted in a median distortion of 0.2 mm for DW-SPLICE, whereas for the conventional method this was 7.2 mm. ADC values, measured using an ice water phantom were in accordance with literature values.
Conclusions: The implementation of DW-SPLICE allows for diffusion-weighted imaging of patients in treatment position with excellent geometrical accuracy. The images can be used to facilitate target volume delineation in RT treatment planning. © *2017 The Authors. Medical Physics published by Wiley periodicals, Inc. on behalf of American Association of Physicists in Medicine.* [https://doi.org/10.1002/mp.12363]

Key words: diffusion, head-and-neck cancer, image distortions, mri, radiotherapy

1. INTRODUCTION

With the increased precision of radiotherapy (RT) treatment delivery, it is becoming increasingly vital to accurately define the target. In head-and-neck (HN) cancer, Computed Tomography (CT) and Magnetic Resonance Imaging (MRI)-based target definition show high interobserver variation. Target volumes determined on CT and MRI are largely overestimated as shown in pathological validation studies.[1,2]

Diffusion-weighted (DW) MRI is a functional imaging technique that provides information on the local mobility of water in tissue. Dense tissues with an increased cellularity, such as glandular and nodal structures or tumors, will restrict the motion of water and show high contrast with surrounding tissue.[3] Due to the high contrast on a DW image between a tumor and its surrounding tissue, DW-MRI shows great potential to facilitate target definition.[4]

The main reason why DW-MRI is not more widely used for target definition in radiotherapy treatment planning of primary tumors is the poor geometrical accuracy of the technique,[5] especially around air cavities. Air-tissue interfaces give rise to strong susceptibility variations which cause large local magnetic field inhomogeneities. Conventional DW-MRI is performed using the single-shot echo planar imaging (EPI) technique, which is very fast and provides a good signal-to-noise ratio (SNR). However, using this EPI technique in the presence of local magnetic field inhomogeneities can lead to image distortions up to centimeters.[5]

To address these susceptibility-induced image distortions, DW-MRI can also be acquired using Turbo Spin Echo (TSE) type imaging sequences. Here, the EPI acquisition module is replaced by a single-shot TSE module, which improves the geometrical accuracy. TSE diffusion has been explored previously in the head-and-neck region for various applications. For the detection and assessment of cholesteatoma, the use of DW-TSE has been investigated rather extensively. Although there does not seem to be consensus on the precise DW-TSE imaging strategy, DW-TSE has been found to have a high predictive and added value.[6,7] DW-TSE methods have also been applied in imaging the salivary glands,[8] the assessment of abscess formation[9] and the differentiation between different types of lesions in the head-and-neck area.[10–12] In head-and-neck cancer, DW-TSE has previously been reported[13–17] to detect and characterize lesions. The majority of the papers applying DW-TSE, report limited experimental details and the image quality is often sub-optimal.

The acquisition of TSE scans is performed under the Carr Purcell Meiboom Gill (CPMG) conditions. These conditions

dictate the timings and phase relations in the sequence. The inclusion of diffusion weighting gradients in a TSE sequence makes that the CPMG conditions are easily violated when subject motion is present. This motion leads to phase errors which will result in destructive interference between spin echoes and stimulated echoes, creating unstable TSE trains and ultimately signal loss or even signal voids in DW-TSE images. Various approaches exist to deal with this issue and create stable echo trains. One is phase cycling of the refocusing pulses in an attempt to preserve the full signal.[18] Another method is echo parity selection, originally proposed by Norris et al.,[19] which aims to separate interfering echo contributions. One echo parity is eliminated by means of an RF pulse[20] or by shifting it out of the acquisition window using an imbalanced readout gradient (U-FLARE[19]). These methods lose a factor of two in signal. The echo parity selection method proposed by Schick,[21] split acquisition of fast spin echo signal for diffusion imaging (SPLICE), is similar to U-FLARE however, both echo parities are acquired and reconstructed separately and afterward their signal magnitudes are combined. The acquisitions are shortened by slightly more than a factor of two to ensure the echo acquisitions do not overlap.[21] This increases the bandwidth, which reduces the sensitivity to distortions even further, but it also lowers the SNR. The resulting SNR is approximately a factor of two lower relative to a comparable CPMG acquisition. So far, only two studies from one research group[13,16] have reported the use of DW-SPLICE in head-and-neck imaging. To improve the image quality, we moved to higher field strength and a dedicated radiotherapy simulation setup, to obtain images with good SNR within an acceptable acquisition time.

In this technical note, we aim to expand upon the existing TSE-based DW sequences by implementing and optimizing the DW-SPLICE sequence at a higher field strength (3.0 T). As these images are meant for target volume delineation prior to radiation treatment in head-and-neck cancer patients, it demands high geometric accuracy.

2. MATERIALS AND METHODS

2.A. MR imaging setup

MR imaging was performed on a 3.0 T wide bore MR system (Ingenia; Philips Healthcare, Best, the Netherlands) using 2-element Flex-M surface coils. Patients were scanned in treatment position using a personalized head support and 5-point head-and-shoulder immobilization mask[22] (Fig. 1).

Measurements were performed on an ice water phantom to validate ADC values. The phantom was built according to Chenevert et al.,[23] a spherical tube filled with demineralized water was inserted in a container filled with ice water. The sequence was tested *in vivo* and a total of 10 patients (seven oropharynx, one larynx, one hypopharynx, and one nasopharynx) were included in the study approved by the institutional review board. These patients received an MRI exam for the purpose of RT treatment planning. We added the DW-SPLICE sequence to this exam.

2.B. MR imaging sequences

Both DW-EPI and DW-SPLICE were performed as a multislice single-shot acquisition using 30 slices of 4 mm. In DW-SPLICE a center-out k-space encoding was used and the refocusing angles were gradually reduced to 60 degrees in the echo train. Diffusion weighting was applied in an isotropic fashion using three orthogonal directions with b-values between 0 and 800 s/mm^2. Fat suppression was executed using spectral presaturation with inversion recovery (SPIR). Both scanning protocols were individually optimized for image quality. Detailed parameters are given in Table I.

A B0 field map was acquired to estimate geometrical accuracy. A 3D gradient echo sequence (flip angle 20°, TE 4.6 ms, ΔTE 2.3 ms, TR 9.5 ms) was used for this. The FOV, voxel sizes and shim settings were the same for both

FIG. 1. MR imaging setup. The patient is positioned using a personalized immobilization mask and head support, surface coils are placed against the sides of the mask. [Color figure can be viewed at wileyonlinelibrary.com]

TABLE I. Sequence parameters used for the pharynx patient imaging. The FOV and related parameters varied slightly for larynx imaging and are denoted in round brackets.

Scan	DW-SPLICE	DW-EPI
FOV (RL × AP × FH) [mm^3]	230 × 280 × 120 (200 × 200 × 120)	230 × 280 × 120 (230 × 230 × 120)
Acquired voxel size [mm^2]	1.8 × 1.8	2.0 × 2.0
Slice thickness [mm]	4	4
TE [ms]	52	63 (61)
TR [ms]	16366 (15844)	3291 (3167)
SENSE acceleration factor	2	2
(Echo) train length [dummies]	64 [1] (55 [1])	69 (57)
Bandwidth [Hz]	900.3 (858.5)	21.4 (26.7)
b-values [s/mm^2] (averages)	0 (2), 800 (5)	0 (2), 50 (2), 100 (2), 200 (2), 500 (4), 800 (6)
Total acquisition time	4 m 38 s (4 m 29 s)	2 m 47 s (2 m 41 s)

diffusion sequences. A gadolinium contrast enhanced T1-weighted TSE multi-acquisition Dixon scan was used as anatomical reference.

An ice water phantom was used to measure ADC values.[23] DW-SPLICE and DW-EPI were acquired on the same scanner and with the same parameters as the patient imaging. The signal intensities from the E_1 and E_2 echo families vary during the initial echoes.[19,21,24] Therefore, an extra acquisition of DW-SPLICE was done using additional (5 total) leading dummy echoes.

2.C. Image evaluation

Image distortions can generally be attributed to gradient nonlinearities, eddy current or magnetic field variations. The gradient nonlinearities are specific for individual MR systems and independent of imaging sequence. The nonlinearities were routinely measured using a specialized phantom for geometric fidelity (Philips Healthcare, Best, the Netherlands). The phantom has a diameter of 55 cm and is measured at seven positions, 7 cm apart, with the central position being the isocenter of the magnet.

Eddy current-related distortions were probed using DW acquisitions of a phantom. The diffusion weighting gradients were applied along the principal axes of the MR system (i.e., using only a single gradient axis per acquisition). The phantom was segmented on the b0 image. This contour was then projected onto the images with a high diffusion weighting in the different directions to visually inspect for geometrical deviations due to eddy currents.

Distortions due to magnetic field variations were investigated using B0 field maps. The acquired B0 field maps were processed using in-house developed software.[5,25] First, phase unwrapping was performed to account for phase wraps in the data. The unwrapped field map was converted to a pixel-shift map using the sequence parameters that dictate the effective spectral width per pixel.[25] Pixel-shift maps were converted to shift-maps in millimeters by multiplication with the voxel dimensions. For DW-EPI, the shifts occur predominantly in the phase encoding direction, while for DW-SPLICE this is the frequency encoding direction. In order to assess the distortions in the relevant areas, the delineated gross tumor volume (GTV), as defined for RT treatment planning, was projected onto the shift-maps. For each GTV, we calculated the median, minimum and maximum shifts over all voxels for both acquisition techniques. The results are given as the median value over all patients and a Wilcoxon signed rank test was used to test for differences.

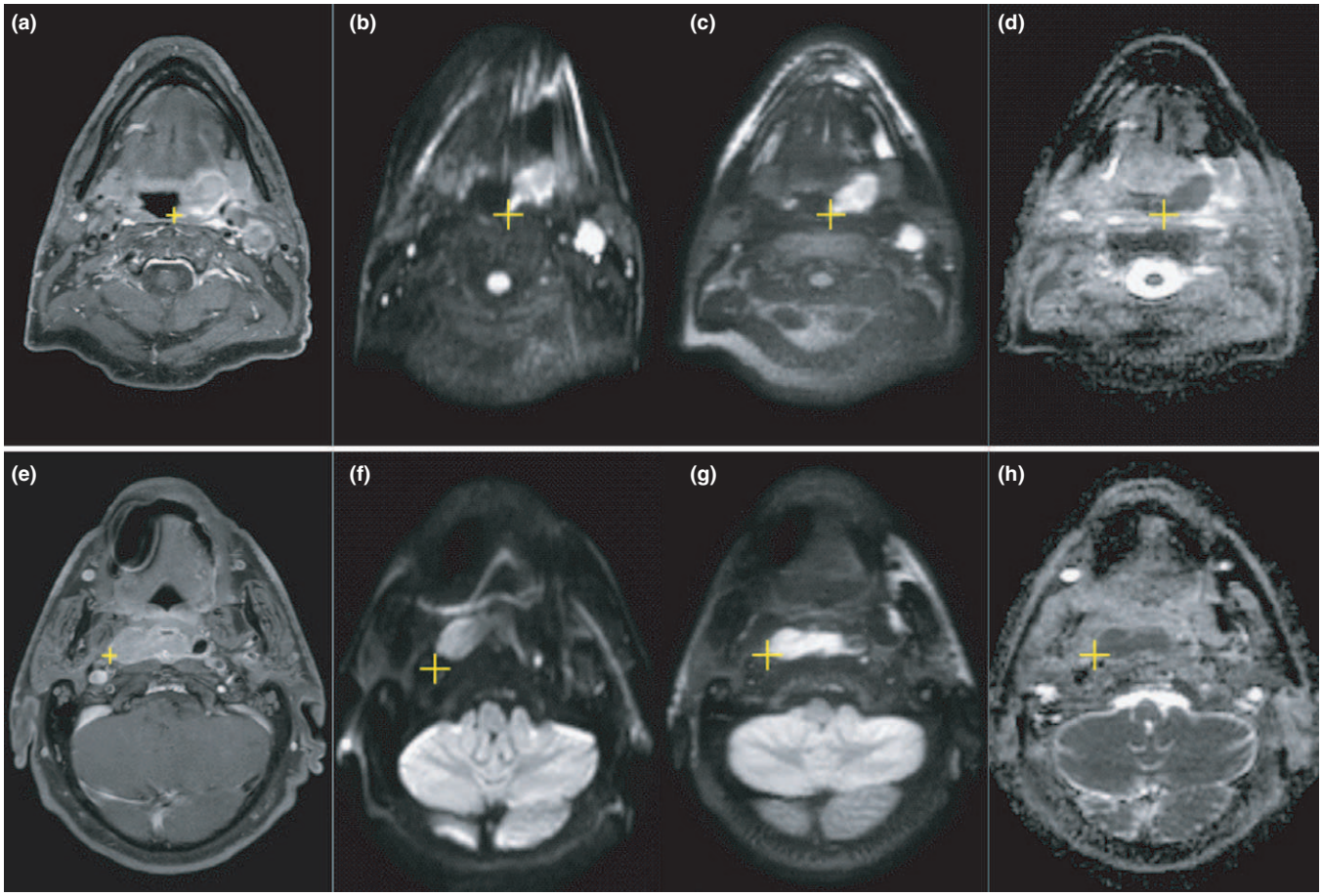

FIG. 2. Examples of DWI in two patients, top row (a)–(d) T2N2b oropharynx, bottom row (e)–(h) T1N0 nasopharynx (with a dental implant causing a signal void). The cursor is linked between different MR scans of the same patient. (a), (e) T1 TSE Dixon, water image, with Gd contrast. (b), (f) DW-EPI b800. (c), (g) DW-SPLICE b800. (d), (h) DW-SPLICE ADC map. [Color figure can be viewed at wileyonlinelibrary.com]

To measure the ADC values, a region of interest (ROI) was defined in the center of the tube in the ice water phantom and this ROI was used to calculate the mean and standard deviation for each technique.

3. RESULTS

3.A. Diffusion-weighted imaging in patients

DWI was successfully acquired in all patients. Two examples, patients 6 and 5 respectively, of the DW images obtained with the two different methods are shown in Fig. 2. The image distortions around the air cavities are immediately recognized in the DW-EPI scans (2b, 2f), while the DW-SPLICE scans (2c, 2g) show the accurate geometry. The diffusion contrast is present in both scans, with the tumor appearing bright on both b800 images and dark on the ADC map. Figure 3 shows the B0 field map with the GTV delineation of the same patient as Figs. 2a–2d. Additional imaging results, B0 field maps and GTV delineations for all patients can be found in Supplementary Figure 1.

3.B. Image distortions

For the MR system used in this study, routine QA measurements of geometric distortions due to gradient nonlinearities were performed. For a central region of at least $25 \times 25 \times 28$ cm^3, which a head-and-neck anatomy does not exceed, the geometric distortions due to gradient nonlinearities were found to be smaller than 1 mm.

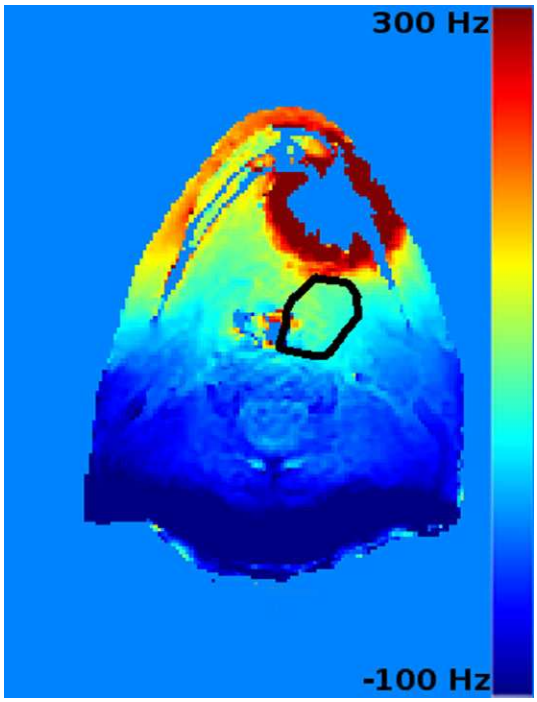

FIG. 3. Example of a B0 field map, same patient as in Figs. 2a–2d. The delineated GTV is indicated with the black line. For this patient, the median distortion was 7.40 mm for DW-EPI and 0.16 mm for DW-SPLICE. [Color figure can be viewed at wileyonlinelibrary.com]

Visual inspection of the phantom contours showed no deviations due to eddy currents in the DW-SPLICE sequence. For DW-EPI, the eddy currents did result in a minor deviation in the outline of the phantom.

Distortion analysis showed that the median shift over all GTVs was 7.2 mm for DW-EPI, with a median minimum and maximum shift of −10.5 mm and 34.9 mm, respectively. While for DW-SPLICE, the median shift over all GTVs was 0.2 mm with a median minimum and maximum shift of −0.3 mm and 1.0 mm, respectively. Additional results for all patients can be found in supplementary Table 1. The difference between the two techniques is statistically significant ($P = 0.002$).

3.C. ADC values

The ice water phantom was scanned with the same sequences as was used for patient imaging [Fig. 4(a)]. The mean ADC of conventional DW-EPI was 1.125 10^{-3} mm^2/s

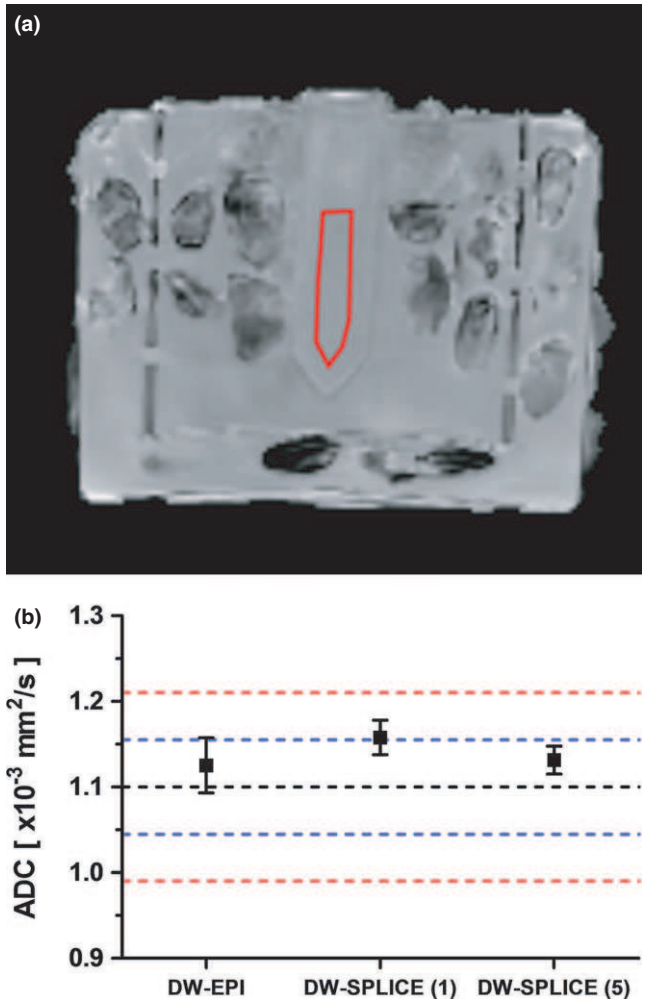

FIG. 4. (a) ADC map of the ice water phantom. The ROI is shown in the center of the phantom. (b) ADC values within the ROI (mean ± standard deviation) of DW-EPI and DW-SPLICE with one and five leading dummy acquisitions. The dashed lines indicate 5 and 10% deviation respectively of the reference value (black dashed). [Color figure can be viewed at wileyonlinelibrary.com]

with a standard deviation of 0.032 10^{-3} mm^2/s. DW-SPLICE yielded 1.158 ($\pm$ 0.020) 10^{-3} mm^2/s. While for DW-SPLICE with additional startup dummies/echoes, the ADC was 1.132 ($\pm$ 0.016) 10^{-3} mm^2/s. For DW-EPI and DW-SPLICE (with additional startup echoes), the ADC values were within 5% of the reported literature value[23] [Fig. 4(b)].

4. DISCUSSION

The main limitation that prevents DW imaging to be widely incorporated in a HN RT treatment planning setting is the poor geometrical accuracy of the conventional DW-EPI acquisition method. The main factor contributing to geometrical distortion in this region is magnetic field inhomogeneity; while the effects of gradient nonlinearity and eddy currents were found to be much smaller. It was shown that when using the DW-SPLICE sequence, the geometrical accuracy is greatly improved. These susceptibility-related distortions were found to be smaller than the acquired voxel size, 0.2 mm vs 1.8 mm for DW-SPLICE. The large difference in the bandwidths of the EPI and TSE sequences already indicates a large intrinsic difference in image distortions. However, as the distortions are related to the magnetic field inhomogeneities, they still need to be evaluated in the relevant area (GTV). The geometric accuracy of DW-SPLICE is comparable to standard anatomical imaging, which allows the diffusion information to be utilized during target volume delineation.

Different methods exist to address the image distortion issue. Techniques such as readout-segmented EPI[26] and reduced FOV imaging[27,28] will increase the bandwidth of the DW-EPI. However, these approaches will not completely eliminate the image distortions as the magnetic field inhomogeneities around the head-and-neck tumors are often so large that an even larger bandwidth is required. Additionally, a reduced FOV approach is often undesirable due to potential lymph node pathology.

The ADC values as measured with the DW-SPLICE sequence in patients are higher than measured with DW-EPI (Fig. 3). During the initial echoes of the echo train of DW-SPLICE, there is still an intensity variation between consecutive echoes.[19,21,24] The addition of more dummy acquisitions at the start of the echo train reduces the intensity variations when the center of k-space is acquired. This will increase TE however, which leads to a reduced SNR. Since we focused on the use of DWI for target delineation, ADC values are used qualitatively to identify T_2 shine through or image artifacts rather than quantitatively. Therefore, we chose to use the acquisition protocol with higher SNR in patients.

The main limitation of the DW-SPLICE sequence is its acquisition speed, a TSE acquisition is inherently slower than EPI. In the presented setup, the acquisition time of a single volume of diffusion data is five times longer for DW-SPLICE (16.4 s) than DW-EPI (3.3 s). This limits the amount of data (e.g., b-values and/or averages) that can be acquired within a clinically acceptable time. DW-SPLICE will also show more blurring in the images due to T_2 relaxation in the echo train of the single-shot acquisition. To decrease the shot length and thus the amount of blurring, dedicated receive coils with more elements could be used to enable higher parallel imaging acceleration factors. This would also speed up the acquisition.

While good fat suppression still remains challenging in this anatomical region, the effects of failing fat suppression in DW-SPLICE are less severe than in DW-EPI. In DW-EPI, unsuppressed fat will suffer from both distortion and large water-fat shift artifacts, causing it to shift through the image and degrade image quality. An example of this is shown in Fig. 2(f). In DW-SPLICE, the unsuppressed fat will not shift and will have less impact on image quality.

The application of DW-SPLICE is not limited to the head-and-neck region and has been applied in other sites as well.[13,29–31] In principle, it can be applied to any anatomical region where conventional DW-EPI suffers from susceptibility-related image distortions. Delineation studies and pathological validation of DW-MRI using DW-SPLICE are subject of future work.

5. CONCLUSION

In conclusion, when compared to DW-EPI, the DW-SPLICE sequence has a significant increase in geometrical accuracy, eliminating image distortions. Using the DW-SPLICE sequence and a dedicated imaging setup at 3.0 T to scan head-and-neck patients in treatment position, we could improve the quality and robustness of DW imaging to facilitate target delineation for RT treatment planning.

ACKNOWLEDGMENTS

The authors thank Gert van Yperen for his help in implementing the diffusion sequence and Ellart Aalbers for providing a picture of the imaging setup. Financial support for this work was provided by the Dutch Cancer Society (project UU 2011-5216).

[a]Author to whom correspondence should be addressed. Electronic mail: t.schakel@umcutrecht.nl; Telephone: 0031 88 7569647.

REFERENCES

1. Caldas-Magalhaes J, Kooij N, Ligtenberg H, et al. The accuracy of target delineation in laryngeal and hypopharyngeal cancer. *Acta Oncol*. 2015;54:1181–1187.
2. Jager EA, Kasperts N, Caldas-Magalhaes J, et al. GTV delineation in supraglottic laryngeal carcinoma: interobserver agreement of CT versus CT-MR delineation. *Radiat Oncol*. 2015;10:26.
3. Thoeny HC, De Keyzer F, King AD. Diffusion-weighted MR imaging in the head and neck. *Radiology*. 2012;263:19–32.
4. Caldas Magalhaes J, Kasperts N, Kooij N, Terhaard C, Raaijmakers C, Philippens M. Validation of diffusion weighted magnetic resonance imaging for automatic tumor delineation in laryngeal cancer. *Int J Radiat Oncol Biol Phys*. 2011;81:S733–S734.
5. Schakel T, Hoogduin JM, Terhaard CH, Philippens ME. Diffusion weighted MRI in head-and-neck cancer: geometrical accuracy. *Radiother Oncol*. 2013;109:394–397.

6. Mas-Estelles F, Mateos-Fernandez M, Carrascosa-Bisquert B, Facal de Castro F, Puchades-Roman I, Morera-Perez C. Contemporary non-echo-planar diffusion-weighted imaging of middle ear cholesteatomas. *Radiographics*. 2012;32:1197–1213.
7. van Egmond SL, Stegeman I, Grolman W, Aarts MC. A systematic review of non-echo planar diffusion-weighted magnetic resonance imaging for detection of primary and postoperative cholesteatoma. *Otolaryngol Head Neck Surg*. 2016;154:233–240.
8. Juan CJ, Chang HC, Hsueh CJ, et al. Salivary glands: echo-planar versus PROPELLER Diffusion-weighted MR imaging for assessment of ADCs. *Radiology*. 2009;253:144–152.
9. Kito S, Morimoto Y, Tanaka T, et al. Utility of diffusion-weighted images using fast asymmetric spin-echo sequences for detection of abscess formation in the head and neck region. *Oral Surg Oral Med Oral Pathol Oral Radiol Endod*. 2006;101:231–238.
10. Chen X, Xian J, Wang X, et al. Role of periodically rotated overlapping parallel lines with enhanced reconstruction diffusion-weighted imaging in correcting distortion and evaluating head and neck masses using 3 T MRI. *Clin Radiol*. 2014;69:403–409.
11. Sakamoto J, Sasaki Y, Otonari-Yamamoto M, Sano T. Comparison of various methods for quantification of apparent diffusion coefficient of head and neck lesions with HASTE diffusion-weighted MR imaging. *Oral Surg Oral Med Oral Pathol Oral Radiol*. 2012;114:266–276.
12. Wang X, Zhang Z, Chen Q, Li J, Xian J. Effectiveness of 3 T PROPELLER DUO diffusion-weighted MRI in differentiating sinonasal lymphomas and carcinomas. *Clin Radiol*. 2014;69:1149–1156.
13. Sakamoto J, Yoshino N, Okochi K, et al. Tissue characterization of head and neck lesions using diffusion-weighted MR imaging with SPLICE. *Eur J Radiol*. 2009;69:260–268.
14. Sakamoto J, Imaizumi A, Sasaki Y, et al. Comparison of accuracy of intravoxel incoherent motion and apparent diffusion coefficient techniques for predicting malignancy of head and neck tumors using half-Fourier single-shot turbo spin-echo diffusion-weighted imaging. *Magn Reson Imaging*. 2014;32:860–866.
15. Verhappen MH, Pouwels PJ, Ljumanovic R, et al. Diffusion-weighted MR imaging in head and neck cancer: comparison between half-fourier acquired single-shot turbo spin-echo and EPI techniques. *AJNR Am J Neuroradiol*. 2012;33:1239–1246.
16. Yoshino N, Yamada I, Ohbayashi N, et al. Salivary glands and lesions: evaluation of apparent diffusion coefficients with split-echo diffusion-weighted MR imaging–initial results. *Radiology*. 2001;221:837–842.
17. Schouten CS, de Bree R, van der Putten L, et al. Diffusion-weighted EPI- and HASTE-MRI and 18F-FDG-PET-CT early during chemoradiotherapy in advanced head and neck cancer. *Quant Imaging Med Surg*. 2014;4:239–250.
18. Le Roux P. Non-CPMG Fast Spin Echo with full signal. *J Magn Reson*. 2002;155:278–292.
19. Norris DG, Bornert P, Reese T, Leibfritz D. On the application of ultra-fast RARE experiments. *Magn Reson Med*. 1992;27:142–164.
20. Alsop DC. Phase insensitive preparation of single-shot RARE: application to diffusion imaging in humans. *Magn Reson Med*. 1997;38:527–533.
21. Schick F. SPLICE: sub-second diffusion-sensitive MR imaging using a modified fast spin-echo acquisition mode. *Magn Reson Med*. 1997;38:638–644.
22. Verduijn GM, Bartels LW, Raaijmakers CP, Terhaard CH, Pameijer FA, van den Berg CA. Magnetic resonance imaging protocol optimization for delineation of gross tumor volume in hypopharyngeal and laryngeal tumors. *Int J Radiat Oncol Biol Phys*. 2009;74:630–636.
23. Chenevert TL, Galban CJ, Ivancevic MK, et al. Diffusion coefficient measurement using a temperature-controlled fluid for quality control in multicenter studies. *J Magn Reson Imaging*. 2011;34:983–987.
24. Dietrich O, Raya JG, Sommer J, Deimling M, Reiser MF, Baur-Melnyk A. A comparative evaluation of a RARE-based single-shot pulse sequence for diffusion-weighted MRI of musculoskeletal soft-tissue tumors. *Eur Radiol*. 2005;15:772–783.
25. Jezzard P, Balaban RS. Correction for geometric distortion in echo planar images from B0 field variations. *Magn Reson Med*. 1995;34:65–73.
26. Foltz WD, Porter DA, Simeonov A, et al. Readout-segmented echo-planar diffusion-weighted imaging improves geometric performance for image-guided radiation therapy of pelvic tumors. *Radiother Oncol*. 2015;117:525–531.
27. Taviani V, Nagala S, Priest AN, McLean MA, Jani P, Graves MJ. 3T diffusion-weighted MRI of the thyroid gland with reduced distortion: preliminary results. *Br J Radiol*. 2013;86:20130022.
28. Wilm BJ, Svensson J, Henning A, Pruessmann KP, Boesiger P, Kollias SS. Reduced field-of-view MRI using outer volume suppression for spinal cord diffusion imaging. *Magn Reson Med*. 2007;57:625–630.
29. Jin N, Deng J, Zhang L, et al. Targeted single-shot methods for diffusion-weighted imaging in the kidneys. *J Magn Reson Imaging*. 2011;33:1517–1525.
30. Burbach JPM, Kleijnen J-PJ, Reerink O, et al. Inter-observer agreement of MRI-based tumor delineation for preoperative radiotherapy boost in locally advanced rectal cancer. *Radiother Oncol*. 2016;118:399–407.
31. Deng J, Omary RA, Larson AC. Multishot diffusion-weighted SPLICE PROPELLER MRI of the abdomen. *Magn Reson Med*. 2008;59:947–953.

SUPPORTING INFORMATION

Additional Supporting Information may be found online in the supporting information tab for this article.

Fig. S1. images from all 10 patients. From left to right: T1w mDixon TSE (water image); DW-SPLICE b800; DW-SPLICE ADC map; DW-EPI b800; DW-EPI ADC map; B0 field map. ADC maps are scaled linearly between 0.0 and 3.0 10^{-3} mm^2/s. The delineated GTV (black line) is projected on the B0 field map

Table S1. B0 distortion analysis of all 10 patients. For each patient, the minimum, median, and maximum image distortion (in mm) is given for both DW-EPI and DW-SPLICE, respectively.